# Facile Synthesis $Cu_2O$ Nanomaterials Via Hydrothermal Method: Effect Of Precursors Ratio On Structural And Morphological Characteristics

Nguyen Thi Tuyet Mai[1*], Luu Thi Lan Anh[2], Luu Thi Hong[3], Ta Ngoc Dung[4], Pham Thanh Huyen[5], Huynh Dang Chinh[5]

[1,4,5,6]*The School of Chemical and Life Science, Hanoi University of Science and Technology, Vietnam; E-mail: mai.nguyenthituyet@hust.edu.vn*

[2]*School of Engineering Physics, Hanoi University of Science and Technology, Vietnam*

[3]*Institute for Building Materials, No. 235 Nguyen Trai, Thanh Xuan, Hanoi, Vietnam*

**Abstracts:** The single phase $Cu_2O$ nanomaterials had been fabricated via facile hydrothermal method using non-toxic precursors of $CuSO_4.5H_2O$ and $Na_2SO_3$ (then, the $CuSO_4$ 0.3M and $Na_2SO_3$ 0.3M solution are mixed with volume ratios of 1:5, 1:6, 1:7 and 1:10, respectively). The observed materials were characterized using fine analysis methods such as X-ray diffraction, scanning electron microscopy, UV-Vis diffuse reflectance spectroscopy, and UV-Vis spectroscopy. The fabricated $Cu_2O$ samples had flower-like morphology which was assembled from octahedrals. The samples had an average crystalline size of ~20.1-23.3 nm and a narrow bandgap of ~1.98 eV. The photocatalytic activity of samples was investigated via Congo red (CR) dye photodecomposition experiment, the catalyst dose and the concentration of CR values were studied as the factors affecting the photocatalytic efficiency. The results showed that the fabricated $Cu_2O$ samples had good photocatalytic ability in decomposing the CR solution in the visible region. The $Cu_2O$ ($M_{1-6}$) sample had the best degradation efficiency of the CR solution was the (reached 91.3% after 300 min under visible light radiation of the 150W Led lamp at the CR concentration of 20 ppm). The photo-decomposition rate constant of $M_{1-6}$ sample reached 0.00774 $min^{-1}$.

**Keywords:** Octahedral $Cu_2O$, flower-like crystals, heterogeneous photocatalysts, Congo red, visible light radiation.

## 1. INTRODUCTION

Cuprous oxide ($Cu_2O$) is known to be a p-type semiconductor with a theoretically narrow direct gap band (Eg≈ 2.17-2.2 eV), which is highly attractive due to the unique properties of the materials. The outstanding advantages of $Cu_2O$ material are non-toxic properties. Raw materials for the production of $Cu_2O$ are available in nature. The $Cu_2O$ fabricated processes are relatively simple and inexpensive [1-7]. Therefore, $Cu_2O$ is one of the fascinating semiconductor materials that is attracting attention in production and application research in many areas such as biosensors, gas sensors, lithium-ion batteries, optoelectronics, luminescence, photocatalysts for air purification, water purification by solar energy, etc. [4-12]. Research works have reported that $Cu_2O$ semiconductor nanomaterials in particular as well as semiconductor nanomaterials in general (ZnO, $TiO_2$, etc.) have been fabricated by various methods such as: thermal oxidation, spray pyrolysis, extraction deposition, laser reduction, microwave, liquid phase synthesis, reduction method, electrochemical method, hydrothermal method, RF sputtering [5-7,13-16]. The sizes and the morphologies (including nanowires, nanoflowers, octahedra, cubes, spheres, hollow spheres, etc.) of nanomaterials depend on the fabrication methods and affect the properties of the material [1,4-7,12-26]. However, the preparation of cuprous oxide nanomaterials with controllable size and morphology to suit designed applications is still an attractive goal for scientists [21-26].

In this report, the nano octahedral $Cu_2O$ p-type semiconductor material was fabricated by a facile hydrothermal method from non-toxic precursor materials - $CuSO_4.5H_2O$ and $Na_2SO_3$. The objective of this research is to investigate the various ratios of precursors on the morphology of the materials as well as the physicochemical properties of the fabricated $Cu_2O$ nanomaterials. The photocatalytic activity of obtained $Cu_2O$ nanomaterials was

characterized via CR decomposing experiment in which the effect photocatalyst dose, CR concentration on photocatalytic activity was also studied and discussed.

## 2. EXPERIMENTS

### 2.1. Synthesis of $Cu_2O$ Nanoparticles

All chemicals were of analytical grade and used without any further purification included of $CuSO_4.5H_2O$ (Merck), $Na_2SO_3$ (99.8%, AR-China), $C_2H_5OH$ (Merck), NaOH (Merck), HCl (Merck), Congo red ($C_{32}H_{22}N_6Na_2O_6S_2$ (CR), 99%, AR-China) and doubly distilled water. A mixed solution consisting of two precursors solutions of $CuSO_4$ 0.3M and $Na_2SO_3$ 0.3M was uniformly stirred with different volume ratios (1:5, 1:6, 1:7 and 1:10) to obtained a green mixed solution. This mixed solution was stirred at room temperature at a constant stirring rate of 350 prm for 30 min, the solution was changed to a light blue color. After that, the mixed solution was transferred to the Teflon line, then put into stainless steel autoclave to perform the hydrothermal process at the temperature of 120 $^oC$ for 24 hours. After the hydrothermal process completed, a paste was obtained which was then filtered, washed by centrifugation three times with distilled water and two times with absolute ethanol until a neutral pH. The washed samples were then dried at 90 $^oC$ overnight in the open-air oven. The obtained products were red-brown fine powders denoted by $M_{1\text{-}5}$, $M_{1\text{-}6}$, $M_{1\text{-}7}$ and $M_{1\text{-}10}$ (with precursors volume ratios 1:5, 1:6, 1:7 and 1:10, respectively).

*Characterizations.* Methods used to determine the properties of materials such as: the X-ray diffraction spectra (XRD, X'pert Pro (PANalytical), Cu-Kα radiation 1.54065 Å, scanning speed 0.03º/2s, scanning angle 2θ≈ 25-75$^o$); the micro-raman spectra (Renishaw Invia Raman Microscope); the scanning electron microscopy (SEM, HITACHI TM4000 Plus); the solid Uv-vis spectra (Jasco V-750) with integrated sphere 60 mm (ISV-922), 200 nm/min and the liquid UV-Vis absorption spectra (Agilent 8453).

### 2.2. Experiment Photocatalytic Activity

The A mixed solution of 0.2 g/L $Cu_2O$ catalyst was added to 50 ml of 20 ppm CR solution in a pyrex beaker. The mixed solution was stirred for 60 min in the dark to reach adsorption-desorption equilibrium. The reaction mixture was then illuminated with the 150 W Led lamp. Periodically according to the reaction time, about 5 ml of the reaction mixture sollution would be taken out for UV-Vis measurements on an Agilent 8453 spectrophotometer at the maximum absorbance of CR dye (496 nm) on the basis of Beer-Lambert law. From that, the remaining concentration of CR in the solution could be determined after each lighting time. The photocatalytic performance was determined via following formula.

$$P= [(C_0-C_t)/C_0]\times 100\% \quad (1)$$

In which, $C_0$ and $C_t$ are CR concentrations at the beginning and at time t during experiment, respectively.

## 3. RESULTS AND DISCUSSIONS

### 3.1. X-ray Diffraction and Raman Shift Spectra Results

Figure 1a presents the X-ray diffraction spectra (XRD) of $M_{1\text{-}5}$, $M_{1\text{-}6}$, $M_{1\text{-}7}$ and $M_{1\text{-}10}$ samples. The XRD results showed that all samples have the similar XRD pattern with the characterizing diffraction peaks at position 2θ with values of 29.6$^o$, 36.4$^o$, 42.45$^o$, 61.5$^o$ and 73.3$^o$. These are assigned to the characteristic peaks of the lattice faces (110), (111), (200), (220) and (311) in octahedral $Cu_2O$ crystal with JCPDS card No 5-669. In addition, there were no diffraction peaks of other phase or impurity that were attributed to Cu and CuO [8,11,13,21]. The Debye-Scherrer equation was applied to calculate the average crystal size at the diffraction peak with the strongest intensity (111) [11,16,21,27,28]. Where d is the average crystal grain size, β is full width half maximum (FWHM) of the peaks, λ is Bragg's angle and λ= 1.54060 Å for CuKα. The average crystal sizes of $M_{1\text{-}5}$, $M_{1\text{-}6}$, $M_{1\text{-}7}$ and $M_{1\text{-}10}$ samples were

determined to be 22.4, 23.3, 21.5 and 20.1 nm, respectively.

$$d= (0.9\times\lambda)/(\beta\times\cos\theta) \qquad (2)$$

Figure 1b exhibits the raman spectra of $M_{1-5}$, $M_{1-6}$, $M_{1-7}$ and $M_{1-10}$ samples. The raman spectra of all samples, the appearance of four peaks at wavenumber 220 $cm^{-1}$, 520 $cm^{-1}$ and 642 $cm^{-1}$, which are assigned to the $2E_u$, $T_{2g}$ and $T_{1u}$(TO) characteristic vibrations of the $Cu_2O$ single-crystal phase natural p-type semiconductor [22,29-32], was clearly observed. In addition, the raman vibrations which are attributed to the CuO or Cu crystalline phase were not found from the raman spectra [29-32]. This showed that the results of the raman spectra were completely consistent with the results from the XRD spectra above.

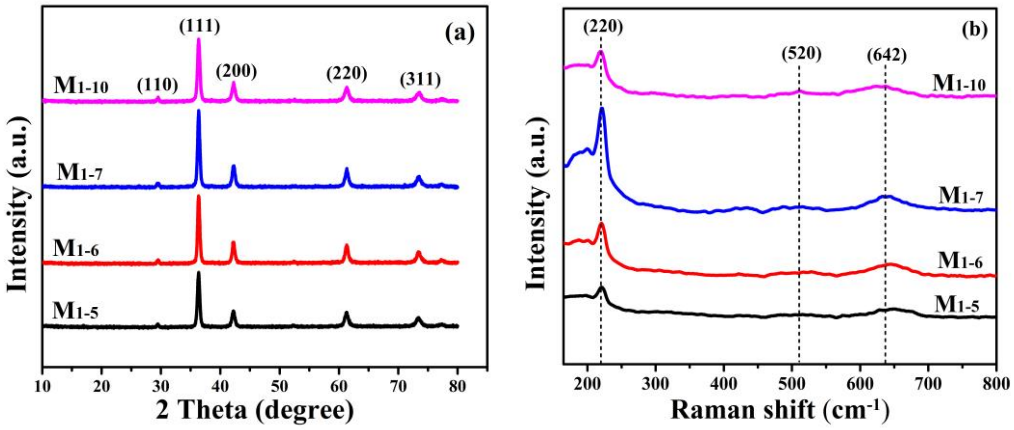


**Figure 1.** a) XRD pattern and b) Raman spectra of $M_{1-5}$, $M_{1-6}$, $M_{1-7}$ and $M_{1-10}$ samples

### 3.2. Scanning Electron Microscopy Results (SEM)

The scanning electron microscopy (SEM) of $M_{1-5}$, $M_{1-6}$, $M_{1-7}$ and $M_{1-10}$ samples were shown in Figure 2. In the SEM images, it was observed that the $Cu_2O$ samples with the $CuSO_4$:$Na_2SO_3$ precursor materials ratio of the 1:5 to 1:10 all have the flower-like morphology. However, the flower-like morphology of the samples were different, from small porosity ($M_{1-5}$ sample) to more porosity ($M_{1-6}$ sample) and almost non-porous or smooth surface ($M_{1-7}$ sample) and the surface with small crystals with thin flakes separated from the bulk crystal surface ($M_{1-10}$ sample) create a distortion of the flower shape (compared to samples with low ratio of $Na_2SO_3$ precursor). Furthermore, in the inserts of $M_{1-5}$, $M_{1-6}$ samples, it was clear that these samples' crystals were octahedra (the part circled by the red circle).

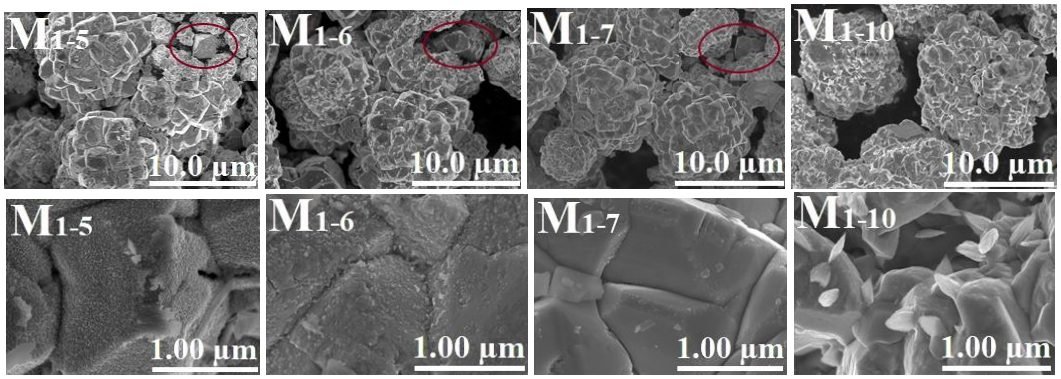


**Figure 2**. Scanning electron microscopy (SEM) of $M_{1-5}$, $M_{1-6}$, $M_{1-7}$ and $M_{1-10}$ samples

At a higher ratio of the initial precursor ($M_{1-7}$ sample), the insert of the $M_{1-7}$ sample showed that the octahedra crystal was slightly distorted (the part circled by the red circle). Meanwhile, in the sample with the highest ratio of the initial precursor ($M_{1-10}$ sample), the octahedra crystal was no longer observed, the crystal was greatly distorted, and at the same time there were a appearance of several thin flake crystals separated from the bulk. This showed a strong influence of initial precursor ratio on the morphology of the composites [4-7,11-12,23-24].

### 3.3. UV-vis Absorption Spectra Results

The solid UV-vis of $M_{1-5}$, $M_{1-6}$, $M_{1-7}$ and $M_{1-10}$ samples were showed in Figure 3a. It was observed in Figure 3a that the samples all had high absorbance (~96%) in the wavelength region of $\lambda \leq 520$ nm, peak absorption at $\lambda \approx 530$ nm (this was consistent with single-crystal phase $Cu_2O$ materials) [2,9]. The absorption was widened at the wavelength region $\lambda \approx$ 530-680 nm and gradually decreased at $\lambda \geq 700$ nm. Based on the solid UV-vis absorption spectra of the fabricated samples (from Figure 3a), the plot of the dependence relationship of $(\alpha h\nu)^2$ versus photon energy $h\nu$ by applying the Tauc equation [2,15,16,22,23,33,34] for the direct p-type semiconductor materials showed in Figure 3b. In Figure 3b, using the extrapolation along the linear line of the plot with the photon energy axis $h\nu$, the Eg bandgap energy of the fabricated samples could be determined. The Eg values of all samples were approximately equal and were reached ≈ 1.98 eV. This Eg bandgap energy value of the fabricated samples, it was found to be suitable for materials with good ability to absorb the light in the visible region [22,23,33,34].

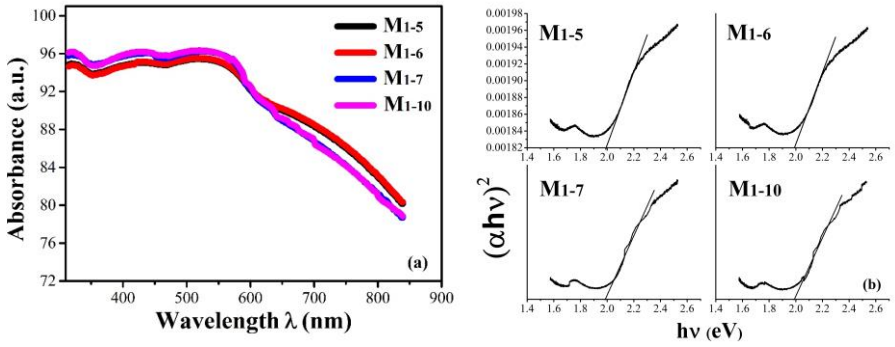


**Figure 3**. a) The solid UV-vis of $M_{1-5}$, $M_{1-6}$, $M_{1-7}$ and $M_{1-10}$ samples; b) The plot of the dependency relationship according to the Tauc equation of $(\alpha h\nu)^2$ versus photon energy $h\nu$

### 3.4. Evaluation of Photocatalytic Properties

+ *Effect of the catalyst dose*. Figure 4a were plots of the photocatalytic activity of $M_{1-5}$, $M_{1-6}$, $M_{1-7}$ and $M_{1-10}$ samples for decomposition of the CR solution under visible light irradiation. Figure 4b was plots of photocatalytic efficiency for the degradation of CR solution of samples after 60 min in dark and 300 min of visible light radiation. The plots in the Figure 4a, Figure 4b showed that, after 60 min in completely dark, the samples achieved photocatalytic efficiency very low of 43.1% except for the $M_{1-6}$ sample had a slightly better efficiency of 44.8%. Next, after 300 min under visible light radiation, the $M_{1-6}$ sample achieved the highest decomposition efficiency of 91.3%. The $M_{1-5}$ and $M_{1-10}$ samples achieved the lowest color degradation efficiency of 79.3%. The $M_{1-7}$ sample achieved the degradation efficiency of 84.5%. Here, it could be seen that a number of factors had affected the photocatalytic performance for degradation the CR dye solution such as: crystallinity, morphology, crystal grain size of the material samples [2,11,21,22,33-39]. Figure 4c showed the rate constant of the photocatalytic reactions which determined based on the Langmuir-Hinshelwood kinetic model according to the plot of the relationship between the $\ln(C_0/C_t)$ function versus time (t) [2,11,34,39]: $\ln(C_0/C_t) = k_{aap}t$ (where $C_0$ and $C_t$ were the initial concentration and the concentration at time t of the reactants, respectively, $k_{aap}$ was the rate constant for the photodegradation reaction of the CR organic dye). The rate constant plots (Figure 4c) showed the values of $\ln(C_0/C_t)$ and reaction time *t* were consistented with the first-order kinetic model with a high $R^2$ correlation coefficient ($R^2 \geq 0.935$). The decomposition

rate constant of $M_{1-6}$ sample was the highest reached 0.00774 $min^{-1}$. The decomposition rate constants of the $M_{1-5}$ and $M_{1-7}$ samples were 0.00470 $min^{-1}$ and 0.00557 $min^{-1}$, respectively. The decomposition rate constant of $M_{1-10}$ sample was the lowest reached 0.00468 $min^{-1}$. It could be seen that the photocatalytic efficiency increased or decreased proportional to the CR colorant decomposition rate constant and the porosity state on the surface of the fabricated samples as observed in SEM figure above (Figure 2). The $M_{1-6}$ sample reached the highest photocatalytic performance for decomposition of pigment at the CR concentration of 20 ppm.

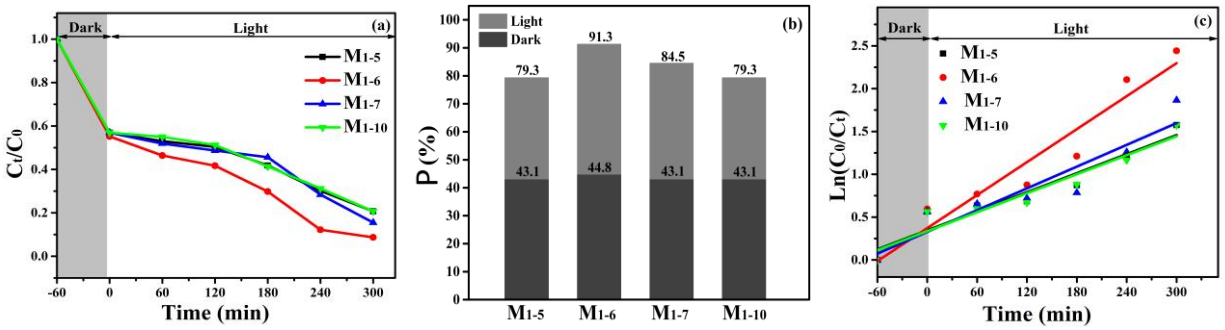


**Figure 4**. a)The degradation of the CR dye solution under visible light radiation; b)The plots of photocatalyst efficiency versus time; c)The photocatalytic kinetics of $M_{1-5}$, $M_{1-6}$, $M_{1-7}$, $M_{1-10}$ samples

+ *Effect of CR pigment concentration.* Figure 5a was a plot to investigate the photocatalytic degradation of $M_{1-6}$ sample in CR solutions with varying concentrations of 10 ppm, 20 ppm, 30 ppm and 50 ppm. Figure 5b was plots of photocatalytic efficiency for the degradation of CR solution of fabricated samples after 60 min in dark and 300 min of visible light radiation which were taken based on the plots of Figure 5a.

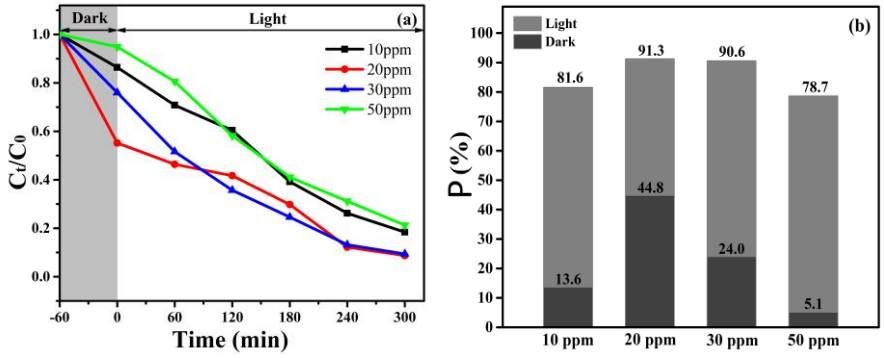


**Figure 5**. a)Investigation of photocatalyst degradation for CR solution with their different concentrations; b)The plots of photocatalyst efficiency of $M_{1-6}$ sample for degradation of the CR different concentration solutions

The plots in the Figure 5a, Figure 5b showed that, when the CR concentration increased the efficiency of the photocatalytic reaction decreased. The highest photocatalytic efficiency was achieved 93.1% (with the CR solution concentration of 20 ppm) and gradually decreased to 78.7% (with the CR solution concentration of 50 ppm). This could be explained by the rate of the reaction was proportional to the dose of catalyst added. However, when the $Cu_2O$ concentration exceeds a limit, the rate of reaction slowed down and became dependent on the $Cu_2O$ concentration. When the photocatalyst content was greater than the limit value, the catalyst particles would be redundant to partially shield the photosensitive surface of the catalyst [2,25].

## CONCLUSIONS

The single-phase $Cu_2O$ nanomaterials were successfully synthesized from $CuSO_4.5H_2O$ and $Na_2SO_3$

precursors via facile hydrothermal method. The morphology of the samples was in flower shape with different surface porosity state and all the fabricated $Cu_2O$ samples showed octahedral crystals shape except for the $M_{1-10}$ sample (octahedral shaped crystals were no longer observed, the crystals were greatly distorted). The fabricated $Cu_2O$ samples all had small crystal sizes of 20.1-23.3 nm with the narrow bandgap energy Eg≈ 1.98 eV calculated by applying the Tauc equation. All these samples had good photocatalytic ability to decompose the CR pigment solution in the visible region. The investigated parameters such as the dose of photocatalyst, the concentration of CR solution were also factors affecting the photocatalytic efficiency. The best CR degradation efficiency reached was the $M_{1-6}$ sample (reached 91.3% after 300 min under visible light radiation of the 150W Led lamp at the CR solution concentration of 20 ppm). The decomposition rate constant of $M_{1-6}$ sample reached 0.00774 $min^{-1}$. These photocatalytic properties for decomposision the above dye solution, it was expected to be had the ability applied in the treatment of contaminated water sources especially in wastewater treatment of the textile-dyeing industry.

## ACKNOWLEDGMENTS

This work was funded by Hanoi University of Science and Technology under the project number CT2022.04.BKA.05, Science and Technology Project of the Ministry of Education and Training of Vietnam. The authors also thank for the support by Hanoi University of Science and Technology under the project number AGF.2022-04.

## REFERENCES

[1] M. Yang, J-J. Zhu, “Spherical hollow assembly composed of $Cu_2O$ nanoparticles, Journal of Crystal Growth”, Journal of Crystal Growth, 256, 134-138, 2003, doi: 10.1016/S0022-0248(03)01298-3.

[2] C.H.B. Ng and W.Y. Fan, “Shape Evolution of $Cu_2O$ Nanostructures via Kinetic and Thermodynamic Controlled Growth”, Journal of Physical Chemistry B, 110, 20801-20807, 2006, doi: 10.1021/jp061835k.

[3] Y. Yang, M. Pritzker, Y. Li, “Electrodeposited p-type $Cu_2O$ thin films at high pH for all-oxide solar cells with improved performance”, Thin Solid Films, 676, 42-53, 2019, doi: https://doi.org/10.1016/j.tsf.2019.02.014

[4] N.T.T. Mai, M.M. Neto, P.V. Thang, N.N. Trung, N.C. Tu, T.N. Dung, H.D. Chinh, L.T.L. Anh, “$Cu_2O$ Nanoparticles: A Simple Synthesis, Characterization and Its Photocatalytic Performance toward Methylene Blue”, Materials Transactions, 61(9), 1868-1873, 2020, doi: 10.2320/matertrans.MT-MN2019039

[5] Y. Dong, Y. Li, C. Wang, A. Cui, Z. Deng, “Preparation of cuprous oxide particles of different crystallinity”, J. Coll. Interface Sci., 243, 85-89, 2001, doi: https://doi.org/10.1006/jcis.2001.7857.

[6] M.A. Shoeib, O.E. Abdelsalam, M.G. Khafagi, R.E. Hammam, “Synthesis of $Cu_2O$ nanocrystallites and their adsorption and photocatalysis behavior”, Advanced Powder Technology, 23, 298-304, 2012, doi: 10.1016/j.apt.2011.04.001.

[7] Y. Luo, S. Li, Q. Ren, J. Liu, L. Xing, Y. Wang, Y. Yu, Z. Jia and J. Li, “Facile Synthesis of Flowerlike $Cu_2O$ Nanoarchitectures by a Solution Phase Route”, Crystal Growth & Design, 7(1), 87-92, 2007, doi: 10.1021/cg060491k.

[8] YS. Li, Q. Lin, X. Liu, L. Yang, J. Ding, F. Dong, Y. Li, M. Irfana and P. Zhang, “Fast photocatalytic degradation of dyes using lowpower laser-fabricated $Cu_2O$–Cu nanocomposites”, Royal Society of Chemistry Advanced, 8, 20277-20286, 2018, doi: 10.1039/c8ra03117g.

[9] S.S. Sawant, A.D. Bhagwat, C.M. Mahajan, “”, Journal of Nano- and Electronic Physics, 8(1), 01035(5pp), 2016, doi: 2077-6772/2016/8(1)01035(5).

[10] Y. Liu, H.K. Turley, J.R. Tumbleston, E.T. Samulski and R. Lopez, “Minority carrier transport length of electrodeposited $Cu_2O$ in ZnO/$Cu_2O$ heterojunction solar cells”, Applied Physics Letters, 98, 162105-1-162105-3, 2011, doi: 10.1063/1.3579259.

[11] R. Inguanta, S. Piazza, C. Sunseri, “Template electrosynthesis of aligned $Cu_2O$ nanowires Part I. Fabrication and characterization”, Electrochimica Acta, 53(22), 6504-6512, 2008, doi: 10.1016/j.electacta.2008.04.075.

[12] Y. Bai, T. Yang, Q. Gu, G. Cheng, R. Zheng, “Shape control mechanism of cuprous oxide nanoparticles in aqueous colloidal solutions”, Powder Technology, 227, 35-42, 2012, doi: 10.1016/j.powtec.2012.02.008.

[13] P. He, X. Shen, H. Gao, “Size-controlled preparation of $Cu_2O$ octahedron nanocrystals and studies on their optical absorption”, Journal of Colloid and Interface Science, 284(2), 510-515, 2005, doi: 10.1016/j.jcis.2004.10.060.

[14] B. Yuana, X. Liua, H. Fub, J. Liua, Q. Zhua, M. Wu, “One-step synthesis of flower-like $Cu_2O$ photoelectric materials by hydrothermal method”, Solar Energy, 188, 265-270, 2019, doi: https://doi.org/10.1016/j.solener.2019.06.014.

[15] J.-Y. Chen, J.-L. Li, P.-J. Zhou, S.-Q. Li, "Depositing $Cu_2O$ of different morphology on chitosan nanoparticles by an electrochemical method", Carbohydrate Polymers, 67(4), 623-629, 2007, doi: 10.1016/j.carbpol.2006.07.003.

[16] M. Hara, T. Kondo, M. Komoda, S. Ikeda, J.N. Kondo, K. Domen, M. Hara, K. Shinohara and A. Tanaka, "$Cu_2O$ as a photocatalyst for overall water splitting under visible light irradiation", Chem. Commun., 3, 357-358, 1998, doi: https://doi.org/10.1039/A707440I.

[17] D.P. Singh, J.A. Singh, P.R. Mishra, R.S. Tiwari, O.N. Srivastava, "Synthesis, characterization and application of semiconducting oxide ($Cu_2O$ and ZnO) nanostructures", Bull. Mater. Sci., 31, 319-325, 2008.

[18] H. Zhang, C. Shen, S. Chen, Z. Xu, F. Liu, J. Li and H. Gao, "Morphologies and microstructures of nano-sized Cu2O particles using a

cetyltrimethylammonium template", Nanotechnology, 16, 267, 2005, doi: 10.1088/0957-4484/16/2/015.

[19] E. Fujii, Y. Kimura, K. Takahashi, M. Furutani, K. Ogura, “Fabrication of Silver Nanoparticles/Chitosan Nanofibers Composite Material Using a High-Pressure Wet-Type Jet Mill and Their Antibacterial Properties”, Materials Transactions, 63(12), 1651-1656, 2022, doi: https://doi.org/10.2320/matertrans.MT-Z2022016.

[20] K. Sato, T. Kuzuya, Y. Hamanaka, S. Hirai, “Synthesis and Analysis of Highly Monodispersed Silver Copper Sulfide Nanoparticles”, Materials Transactions, 62(6), 731-737, 2021, doi: https://doi.org/10.2320/matertrans.MT-M2020395.

[21] Z. Zheng, B. Huang, Z. Wang, M. Guo, X. Qin, X. Zhang, P. Wang and Y. Dai, “Crystal Faces of $Cu_2O$ and Their Stabilities in Photocatalytic Reactions”, Journal of Physical Chemistry C, 113(32), 14448-14453, 2009, doi: 10.1021/jp904198d.

[22] M. Singha, D. Jampaiaha, A.E. Kandjani, Y.M. Sabrib, E.D. Gasperac, P. Reineckd, M. Judde, J. Langleye, N. Coxe, J.V. Emdbenc, E. Mayesf, B.C. Gibsond, S.K. Bhargavab, R. Ramanathana, V. Bansal, “Oxygen-deficient photostable $Cu_2O$ for enhanced visible light photocatalytic activity”, The Royal Society of Chemistry, 1-3, 1-13, 2013, doi: 10.1039/C7NR08388B.

[23] X. Yu, L. Huang, Y. Wei, J. Zhang, Z. Zhao, W. Dai, B. Yao, “Controllable preparation, characterization and performance of $Cu_2O$ thin film and photocatalytic degradation of methylene blue using response surface methodology”, Materials Research Bulletin, 64, 410-417, 2015, doi: http://dx.doi.org/10.1016/j.materresbull.2015.01.009.

[24] S-K. Li, X. Guo, Y. Wang, F-Z. Huang, Y-H. Shen, X-M. Wanga and A-J. Xie, “Rapid synthesis of flower-like $Cu_2O$ architectures in ionic liquids by the assistance of microwave irradiation with high photochemical activity”, Dalton Transactions, 40, 6745-6750, 2011, doi: 10.1039/c0dt01794a.

[25] S. Rasheeda, Z. Batoolb, A. Intisarc, S. Riazd, M. Shaheena, R. Kousar, “Enhanced photodegradation activity of cuprous oxide nanoparticles towards Congo red for water purification”, Desalination and Water Treatment, 227, 330-337, 2021, doi: 10.5004/dwt.2021.27238.

[26] M. Basu, A.K. Sinha, M. Pradhan, S. Sarkar, A. Pal, C. Mondal and T. Pal, “Methylene Blue−$Cu_2O$ Reaction Made Easy in Acidic Medium”, Journal of Physical Chemistry, C 116, 25741-25747, 2012, doi: 10.1021/jp308095h.

[27] M.A. Khan, M. Ullah, T. Iqbal, H. Ahmood, A.A. Khan, M. Shafique, A. Majid, A. Ahmed, N.A. Khan, “Surfactant Assisted Synthesis of Cuprous Oxide ($Cu_2O$) Nanoparticles via Solvothermal Process”, Nanosci. and Nanotech. Research, 3(1), 16-22, 2015.

[28] S.A. Rastabi, J. Moghaddam, M.R. Eskandarian, “Synthesis, characterization and stability of $Cu_2O$ nanoparticles 3 produced via supersaturation method considering operational 4 parameters effect”, Journal of Industrial and Engineering Chemistry, 22, 34-40, 2015, doi: http://dx.doi.org/10.1016/j.jiec.2014.06.022.

[29] Y. Deng, A.D. Handoko, Y. Du, S. Xi and B.S. Yeo, “In Situ Raman Spectroscopy of Copper and Copper Oxide Surfaces during Electrochemical Oxygen Evolution Reaction: Identification of CuIII Oxides as Catalytically Active Species”, ACS Catalysis, 6, 2473-2481, 2016, doi: 10.1021/acscatal.6b00205.

[30] K. Dharmalingam, D. Bordoloi, A.B. Kunnumakkara, R. Anandalakshmi, “Preparation and characterization of cellulose-based nanocomposite hydrogel films containing CuO/$Cu_2O$/Cu with antibacterial activity”, Journal of Applied Polymer Science, e49216, 1-14, 2020, doi: 10.1002/app.49216.

[31] M.G. Rahimi, A. Wang, G. Ma, N. Han and Y. Chen, “A one-pot synthesis of a monolithic $Cu_2O$/Cu catalyst for efficient ozone decomposition”, RSC Advances, 10, 40916-40922, 2020, doi: 10.1039/d0ra05157h.

[32] J. Benz, K.P. Hering, B. Kramm, A. Polity, P.J. Klar, S.C. Siah and T. Buonassisi, “The influence of nitrogen doping on the electrical and vibrational properties of $Cu_2O$”, Physica Status Solidi B, 1-5, 2016, doi: 10.1002/pssb.201600421.

[33] N. Helaïli, Y. Bessekhouad, A. Bouguelia, M. Trari, “Visible light degradation of Orange II using x$Cu_yO_z$/$TiO_2$ heterojunctions”, Journal of Hazardous Materials, 168, 484-492, 2009, doi: 10.1016/j.jhazmat.2009.02.066.

[34] Y. Luo, S. Li, Q. Ren, J. Liu, L. Xing, Y. Wang, Y. Yu, Z. Jia, and J. Li, “Facile Synthesis of Flowerlike $Cu_2O$ Nanoarchitectures by a Solution Phase Route”, Crystal Growth & Design, 7(1), 87-92, 2007, doi:

[35] J. An, Q. Zhou, “Degradation of some typical pharmaceuticals and personal care products with copper-plating iron doped $Cu_2O$ under visible light irradiation**”**, Journal of Environmental Sciences, 24(5), 827-833, 2012, doi: 10.1016/S1001-0742(11)60847-4.

[36] Y. Zhang, B. Deng, T. Zhang, D. Gao and A-W. Xu, “Shape Effects of $Cu_2O$ Polyhedral Microcrystals on Photocatalytic Activity”, Journal of Physical Chemistry, C 114, 5073-5079, 2020, doi: 10.1021/jp9110037.

[37] X. Yu, K. Song, J. Nie, J. Zhang, Y. Wei, J. Niu and B. Yao, “Preparation and performance of $Cu_2O$/$TiO_2$ nanocomposite thin film and photocatalytic degradation of Rhodamine B”, Water Science and Technology, 1-12, 2018, doi: 10.2166/wst.2018.369.

[38] B. Qin, Y. Zhao, H. Li, L. Qiu, Z. Fan, “Facet-dependent performance of $Cu_2O$ nanocrystal for photocatalytic reduction of Cr(VI)”, Chinese Journal of Catalysis, 36(8), 1321-1325, 2015, doi: https://doi.org/10.1016/S1872-2067(15)60877-4.

[39] Y. Dong, F. Tao, L. Wang, M. Lan, J. Zhang and T. Hong, “One-pot preparation of hierarchical $Cu_2O$ hollow spheres for improved visible-light photocatalytic properties”, RSC Advances, 10, 22387-22396, 2020, doi: 10.1039/d0ra02460k.

DOI: https://doi.org/10.15379/ijmst.v10i5.2469